Tumor Spheroids Layered in an Imageable Cancer Environment (T-SLICE): a novel *in vitro* platform to study tumor biology

Authors/Affiliations:

Morgan Pugh-Toole[*1,2], Nicholas Dawe[*2,3], Jeanette E. Boudreau[1,2,4], Brendan M. Leung[1,2,3,5]

[1]Department of Pathology, Dalhousie University

[2]Beatrice Hunter Cancer Research Institute

[3]School of Biomedical Engineering, Dalhousie University

[4]Department of Microbiology & Immunology, Dalhousie University

[5]Department of Applied Oral Sciences, Dalhousie University

Correspondance: Dr. Brendan Leung, bleung@dal.ca

Mailing Address: 5891 University Avenue, Dentistry Building, Room 5193, Halifax, NS, B3H 1W2

*These authors contributed equally to the manuscript.

Keywords: Tumor Microenvironment, 3-D culture system, hypoxia, microscopy

Summary

Cancer treatment is shifting away from traditional to precise therapeutic approaches informed by patient and tumor profiles. To achieve better outcomes for cancer patients, it will be necessary to design and test therapies that target the heterogeneity of tumors that exists within and between patients and even within the same tumor. Existing *in vitro* model systems do not fully recapitulate the physio-chemical gradients of tumors and may fall short of representing a living organism. Mouse models remain the gold standard for preclinical testing but lack the throughput needed to quickly understand mechanisms and iterate quickly to maximize therapeutic efficacy. Microfluidic systems can fill this gap but remain out of reach for most biologic laboratories due to their complexity in assembly and use. We created T-SLICE (Tumor Spheroids Layered in an Imageable Cancer Environment) to enable high-throughput imageable studies within a complex simulated tumor microenvironment (TME). Tumor spheroids are seeded on a monolayer of fibroblasts and cultured between two parallel, closely spaced glass coverslips (300-700 μm). The restrictive gap distance limits permeation of nutrients and oxygen to create gradients that recapitulate those observed in the *in vivo* TME. In T-SLICE, physio-chemical gradients are defined by cellular metabolism, akin to an actual tumor. We demonstrate that this is associated with changes in cellular viability, mitochondrial trans-membrane potential, and proliferation. T-SLICE provides a live-cell imaging compatible, high throughput platform that allows real-time monitoring of cellular phenotypes, function, and sociology within a cell-driven TME physio-chemistry amenable to therapeutic optimization, screening, and patient avatar modelling.

42 **Introduction**

43 Tumors are dynamic communities of cells that together form a microenvironment with gradients
44 of nutrient and oxygen availability[1]. Within the tumor microenvironment (TME), the relative
45 frequencies of stromal and tumor cells can vary, impacting tumor progression and prognosis[2].
46 Research has begun to uncover the dynamic nature of the TME and physio-chemical factors that
47 allow cancer cells to persist and invade healthy tissues, but model systems have not allowed
48 faithful recapitulation of these complex TMEs[1,3].

49 The hypoxic cellular response is of particular significance as it is implicated in both DNA
50 damage and repair and apoptosis of malignant cells[4]. Acute hypoxic responses lead to the
51 accumulation of reactive oxygen species (ROS), leading to DNA damage, and chronic hypoxia
52 leads to impairments in DNA damage repair. Over time, such responses in cancer cells can lead
53 to the accumulation of irreparable DNA mutations and give rise to advanced malignancies[5]. Cell
54 metabolism within the TME generates physio-chemical gradients that increase with tumor size
55 and availability of blood supply, compounded by relatively poor vascularization and reduced
56 ability of oxygen and nutrients to diffuse through the tumor[6]. A nutrient-poor, hypoxic core that
57 favors anaerobic metabolism is established as a result. Tumor cells persisting in these conditions
58 must adapt, which often manifests as decreased proliferation, increased mutation rates, and
59 resistance to apoptosis[6,7].

60 The heterogeneous TME drives diversification of cancer cell phenotypes, making it
61 unlikely that a single intervention will completely eradicate the tumor. Using mainstream drug
62 development pipelines, oncology drug candidates promising in preclinical trials have a low
63 probability of success by the time they reach phase III clinical trials, with a cumulative failure
64 rate of approximately 97%[8]. Immunotherapies are showing promise for treating solid tumors, but

most patients still fail to achieve long-term durable responses[9]. Likely, these studies reflect that most tumors are only partially sensitive to therapeutic interventions because their diversity is underestimated in existing preclinical models. Strategies to experimentally recapitulate the complex TME are urgently required.

To enable high-throughput and mechanistic studies that recapitulate the TME, we created Tumor Spheroids Layered in an Imageable Cancer Environment (T-SLICE). The T-SLICE culture model is designed to be compatible with standard life science laboratory techniques. T-SLICE incorporates tunable physio-chemical parameters to recreate specific features of the TME of different malignancies for experimental study. In T-SLICE, a fibroblast monolayer is seeded with tumor spheroids between two glass coverslips with a narrow vertical gap (300-700 μm). The small gap space negates most convective transport caused by bulk fluid flow, creating a diffusional resistance that is inversely proportional to its height. As a result of metabolism, cells closer to the edge of the parallel glass coverslips preferentially receive oxygen; thus, a hypoxic gradient is formed from the periphery toward the middle of the T-SLICE. The monolayer of fibroblasts seeded within the gap creates a gradient profile that simulates a TME of a tumor the same size as the coverslip. By adding small spheroids within the gap space, we address the shortcomings of conventional spheroid culture because we uncouple tissue architecture from metabolically-generated physio-chemical gradients. T-SLICE enables control of physio-chemical gradients independently from tumor tissue density, allowing live imaging of the hypoxic region of the TME, and therefore empowers laboratories to better test interventions in a faithful *in vitro* system.

87 **Methods**

88 *3-D mold design and printing*

89 T-SLICE design and construction are depicted in Figure 1A-B. T-SLICE chips were designed
90 using Autodesk® Fusion 360™ Computer-Aided Design (CAD) software as '.stl' files, then
91 converted to '.ctb' files using Chitubox® 3-D printing preprocessing software. Designs were 3-D
92 printed using an ELEGOO Mars 2 Pro MSLA 3-D Printer (ELEGOO, Shenzhen. China). Molds
93 were created from Standard LCD UV-Curing Photopolymer Rapid Resin (ELEGOO, Shenzhen.
94 China) in 0.05mm layers, each cured by 6 seconds of UV light exposure (405nm). Resin molds
95 were washed in isopropanol (20 min) and UV-cured (405 nm, 30 min) (ELEGOO Mercury Plus
96 Washing and Curing Machine, Shenzhen. China). Uncured resin monomers were extracted from
97 molds by soaking in 95% ethanol (3x24h, room temperature, with agitation).

98 T-SLICE chips were prepared by pouring Polydimethylsiloxane (PDMS) (10:1 elastomer
99 to curing agent, Sylgard 184™ Silicone Elastomer Kit, Corning) into the resin molds, degassed
100 in a vacuum chamber for 15 min, then cured (60° for 24 h) and removed using forceps. A No. 1
101 18mm coverslip was covalently bonded to the underside of the chip by plasma oxidation (1-2
102 min.). Before use in cell culture, T-SLICE chips were sterilized in 70% ethanol and exposed to
103 UV light for 30 min.

104

105 *Cell Culture*

106 The NIH/3T3 (fibroblast), MCF-7 (breast cancer), and HCC-1806 (breast cancer) cell lines were
107 obtained from the American Type Culture Collection (ATCC), and the ID8 *Trp53*$^{-/-}$ (ovarian
108 cancer) cell line was generously gifted by Dr. Madhuri Koti (Queen's University). Cells were
109 maintained in a humidified incubator at 37°C and 5% CO_2. MCF-7 and NIH/3T3 cells were

110 maintained Dulbecco's Modified Eagle Media (DMEM; Gibco) supplemented with 10% fetal
111 bovine serum (FBS; Gibco) and 1% antibiotic-antimycotic (AA;100 IU/mL penicillin, 0.1
112 mg/mL streptomycin and 0.25 µg/mL amphotericin-B, Gibco,). HCC-1806 cells were maintained
113 in RPMI-1640 media (Gibco) supplemented with 10% FBS and 1% AA. ID8-*Trp53*$^{-/-}$ cells[10]
114 were maintained in DMEM supplemented with 10% FBS, 1% penicillin-streptomycin (PS;
115 Wisent), and 1% Insulin Transferrin Selenite (ITS; Wisent)[10].
116
117 *Spheroid culture in 384-hanging drop plates and T-SLICE assembly*
118 Tumor spheroids were created using Perfecta3-D™ 384-well hanging drop culture plates (3-D
119 Biomatrix Inc. Ann Arbor, MI). Before seeding, plates were pretreated in 0.1% w/v Pluronic® F-
120 108 solution (Sigma-Aldrich) in distilled water, then rinsed with distilled water and UV-
121 sterilized for 30 min. MCF-7 (50 cells) or HCC1806 and ID8-*Trp53-/-* (100 cells) were seeded in
122 25 µL droplets containing culture media supplemented with 2.4 mg/mL MethoCel® A4M
123 (Sigma-Aldrich) to create spheroids with diameters of approximately 150 µm. To prevent
124 spheroid merging, droplets were seeded in a lattice pattern, yielding 192 spheroids for each 384-
125 well hanging drop plate. Spheroids were maintained under standard cell culture conditions
126 (37°C, 5% CO_2). Following spheroid formation (24h for MCF-7; 48h for HCC1806 and ID8-
127 *Trp53-/-*), cells were pooled and seeded onto fibroblast monolayers in T-SLICE.
128 T-SLICE culture is assembled within a standard six-well cell culture-coated plate.
129 NIH/3T3 fibroblasts are cultured on autoclaved No. 1 18mm round coverslips (VWR) pretreated
130 with fibronectin (10 µg/mL in PBS; Sigma-Aldrich) for 45 min. Coverslips are with NIH/3T3
131 fibroblasts overnight at 200,000 cells per coverslip (400,000 cells/mL), incubated overnight to
132 reach confluency, and then seeded with 192 spheroids/coverslip. Spheroids were collected,

133 centrifuged at 200 x *g*, and resuspended in 500 µL of complete cell culture media, which was
134 then used to replace the culture media atop the fibroblasts. Fibroblasts and spheroids were co-
135 cultured overnight, then the T-SLICE chip was placed, and 2mL of cell culture media was added
136 to the sides until the area under the chip was filled by capillary action. Media was changed in
137 500µL increments every 24h. Control wells without T-SLICE were cultured in parallel. Zones of
138 T-SLICE were defined as middle, intermediate and peripheral zones, representing concentric
139 rings of 0-3mm, 3-6mm or 6-9mm diameter, respectively.
140
141 *EF5 for characterization of hypoxic responses within T-SLICE of MCF-7, HCC1806 and ID8*
142 *Trp53-/- cells*
143 To characterize hypoxic cellular responses, we cultured T-SLICE in the presence of 100 µM of
144 the EF5 Hypoxia Detection Kit (Sigma-Aldrich). Cell culture media was supplemented with 100
145 µM EF5 incorporated into the media for 6, 12, 24, or 48 h. EF5 (2-(2-Nitro-1H-imidazol-1-yl)-
146 N-(2,2,3,3,3-pentafluoropropyl) acetamide), is a 2-nitroimidazole compound that is reduced in
147 hypoxic cells to form adducts at the cell membrane that can be fluorescently labelled with a
148 fluorophore-conjugated anti-EF5 antibody[11]. After the T-SLICE chip was removed, cells were
149 fixed in 4% paraformaldehyde in PBS overnight at 4°C. Cells were then washed and prepared for
150 imaging according to the manufacturer's instructions, using the anti-EF5, clone ELK3-51
151 Cyanine 3 conjugate mouse monoclonal antibody (5µg/mL in 1% BSA/PBS; Sigma-Aldrich).
152 Imaging was done with the EVOS™ Light Cube, RFP 2.0 (Ex: 542 nm; Em: 593nm).
153
154
155

156 *Measuring cellular proliferation using the EdU Cell Proliferation Kit*

157 Cell proliferation in T-SLICE zones was analyzed using an EdU (5-ethynyl-2'-deoxyuridine)
158 Cell Proliferation Kit (Click-iT™ EdU Cell Proliferation Kit for Imaging, Alexa Fluor™ 488
159 dye: Invitrogen). Cell culture media was supplemented throughout with 10 uM EdU. After 72h,
160 T-SLICE chips were removed, and the cells were fixed with 4% paraformaldehyde (PFA)
161 solution in PBS for 15 min at RT, then stained according to the manufacturer's instructions.
162 Imaging was performed using the EVOS™ Light Cube, GFP 2.0.

163

164 *Assessment of cell viability using Calcein-AM and ethidium homodimer-1*

165 Imaging was performed on the EVOS™ FL Auto 2 Cell Imaging System, all assessed with
166 ImageJ. Viability of cells cultured within T-SLICE was assessed using Calcein-AM
167 (ThermoFisher Scientific) to label live cells and ethidium homodimer-1 (EthD; Invitrogen) to
168 label dead cells. At specified timepoints, T-SLICE chips were removed, cells washed once with
169 PBS, and stained with a 1μM Calcein-AM, 1 μM ethidium homodimer-1 solution in PBS for 30
170 min at room temperature (RT) in the dark. Cells were washed twice with 1 mL PBS and then
171 immersed in PBS for imaging using the EVOS™ Light Cube, GFP 2.0 (Ex: 482 nm, Em: 524
172 nm) and EVOSTM Light Cube, RFP 2.0 (Ex: 542 nm, Em: 593 nm).

173 *Measuring Mitochondrial Membrane Potential using MitoView 633*

174 MitoView™ 633 (Biotium) was used to measure mitochondrial membrane potential (MMP)
175 according to the manufacturer's recommendation. Cell culture media was supplemented with 100
176 nM MitoView 633 (Biotium) for the duration of T-SLICE culture. Live T-SLICE cultures were
177 imaged every 24h using the EVOS™ Light Cube, Cy5 2.0 (Ex: 635 nm, Em: 692 nm).

178

179 *Statistical analysis*

180 Statistical analysis of data was performed using GraphPad Prism 9 (GraphPad Software). Two-

181 way analysis of variance (ANOVA) with Tukey's multiple comparisons test was performed to

182 assess multi-group comparisons. *P*-values are represented as follows: $*p<0.05$; $**p<0.01$;

183 $***p<0.001$; $****p<0.0001$.

184

185 **Results**

186 *Design and optimization of T-SLICE*

187 We sought to create a synthetic TME that recapitulates the physio-chemical properties of a solid
188 tumor, focusing on oxygen tension and mitochondrial stress. We iterated on design, considering
189 both ease of device fabrication and experimental use. Chip geometry, cell growth surface area,
190 and distance between the two parallel-spaced glass coverslips are all factors that can influence
191 the biochemical gradients within T-SLICE and were therefore considered together during
192 conceptualization and design. Circle and square geometries were evaluated using prototypes with
193 gap heights ranging from 300-700 µm. In comparison to squares, circular geometry has a
194 symmetrical center-to-edge distance for easier measurement of cell distances. To recapitulate
195 tumor microenvironments with different oxygen tensions, we created T-SLICE chips with a
196 range of gap heights **(Figure 1A, B).** For the current study, we chose a circular design using an
197 18mm glass coverslip bonded on the underside of a PDMS chip of 24 mm diameter and 4 mm
198 total height. Three different T-SLICE chip gap heights of 300 µm, 500 µm, or 700 µm were
199 created and placed on top of a bottom coverslip, between which cells are cultured.

200 Fibroblasts are a prominent cell type found in the stromal region of tumors and play an
201 essential role within the TME. To capture aspects of the TME within T-SLICE, we used
202 NIH/3T3 embryonic murine fibroblasts as the gradient-driving monolayer. On an 18 mm
203 coverslip within a 6-well plate, we grew NIH/3T3 cells to confluency and seeded tumor
204 spheroids. We tested a range of cell seeding densities and found that $2x10^5$ NIH/3T3 cells best
205 established a confluent monolayer in 24h, onto which tumor spheroids could be supported
206 without direct contact with the coverslip and any associated deformation due to spheroid
207 adhesion spreading **(Figure 1C)**. In parallel, we optimized cancer cell seeding densities in

208 hanging drop culture to create spheroids with a diameter <150 µm. We chose this limit to
209 exclude the possibility of generating internal physio-chemical gradients and to ensure that the
210 hypoxia level of a given spheroid is dependent only on its position under the T-SLICE chip. The
211 small size of the spheroid further allows imaging and microscopic detection and quantification of
212 changes within it, as confirmed using brightfield microscopy (**Figure 1C**).
213
214 *T-SLICE culture generates sustained hypoxic gradients*
215 Hypoxia is a hallmark biochemical pressure within heterogeneous TME of solid tumors that
216 results from cellular oxygen consumption and limited availability, especially in regions distal to
217 the blood supply[12]. We expected that hypoxia would occur most prominently at the center of the
218 T-SLICE. To assess this, we identified three concentric zones for analysis: middle (M, 0– 3 mm
219 from centre), intermediate (I, 3– 6 mm from centre), and periphery (P, 6– 9 mm from centre).
220 Using EF5 staining, we measured hypoxia within T-SLICE after 6, 12, 24 and 48h of culture. At
221 all three gap heights tested, increasing time resulted in greater hypoxia among MCF7 cells
222 ($p<0.0001$, **Figure 2**); this result was confirmed in a second cell line, HCC1806
223 (**Supplementary Figure 1**). For all cell lines and gap heights tested, EF5 fluorescence intensity
224 was highest in the middle zone of T-SLICE and progressively decreased in the intermediate and
225 peripheral zones. EF5 staining was observed as early as 6 h and increased during the 48h during
226 which we studied cells in T-SLICE for this experiment ($p<0.00-5$ for all gap heights). Hypoxic
227 reactions were most pronounced with the smallest gap height (300 µm) compared to the larger
228 gap heights, consistent with our prediction of decreasing oxygen availability with restricted
229 diffusion as gap height decreases ($p<0.0001$ at all timepoints). Together, our results indicate that

230 T-SLICE functions to establish cell-driven hypoxic gradients that can be tuned by altering gap
231 heights.
232
233 *Cellular proliferation is diminished in the hypoxic regions of T-SLICE*
234 A direct impact of hypoxia in cancer cells is the reduction of proliferation to maintain viability[12].
235 We next used the EdU assay to assess whether cellular proliferation is diminished in the hypoxic
236 regions of T-SLICE. After 72h of culture, proliferation of tumor cells within spheroids and
237 fibroblasts was most present in the peripheral zone of T-SLICE **(**$p<0.0001$, **Figure 3 and**
238 **Supplementary Figure 2)**. Newly divided MCF-7 or HCC1806 cells were not detected in the
239 middle zone, at any gap height. In MCF7 cells, cell proliferation increased with higher gap
240 heights ($p<0.001$), confirming that cellular proliferation and hypoxia are inversely related in T-
241 SLICE.
242
243 *Cell viability is reduced in the hypoxic regions of T-SLICE*
244 Concurrent with reduced proliferation, loss of cell viability is commonly observed in hypoxic
245 regions due to deprivation of essential nutrients and oxygen[12]. To examine cellular viability
246 within T-SLICE zones, we cultured cells for 72 h and used Calcein-AM and ethidium
247 homodimer-1 to stain in tandem to identify live (green) and dead (red) cells, respectively **(Figure**
248 **4)**. Cell viability was near 100% in the peripheral zone of T-SLICE at all gap heights tested. In
249 MCF-7 spheroids cultured with 300 µm gap height, cell viability dropped to ~50% and ~0% in
250 the intermediate and middle zones, respectively, but this diminution was nearly completely
251 abrogated when gap heights were raised to 500 µm and 700 µm. We observed similar cell
252 viability trends when we instead used ID8 *Trp53-/-* cells in T-SLICE (Supplemental Figure 3).

253 *Hypoxia, slowed proliferation and cell death in T-SLICE is associated with loss of mitochondrial*
254 *membrane potential*
255 Loss of mitochondrial trans-membrane potential MMP is a characteristic early feature of
256 apoptosis and can be brought about by hypoxic stress[13]. MitoView 633 was used to analyze the
257 mitochondrial membrane potential of cancer cells cultured in T-SLICE for up to 48h **(Figure 5**
258 **and Supplementary Figure 4)**. In both MCF-7 and ID8 *Trp53-/-* cells, MMP was significantly
259 diminished in the intermediate and middle zones of T-SLICE compared with the periphery
260 ($p<0.001$). This impact was significantly greater after 48h ($p<0.001$). Altogether, our results
261 indicate that T-SLICE greats physio-chemical gradients of hypoxia that correspond to loss of
262 cellular transmembrane potential, impacting cellular viability and proliferation.
263

264 **Discussion**

265 Hypoxia is a characteristic of tumors, whose rapid growth often outpaces by blood vessel
266 formation[14]. The limitation in oxygen, nutrients, and waste removal force tumor cells to adapt
267 their metabolic features or undergo apoptosis. These adaptations are associated with increased
268 metastasis, genomic instability, treatment resistance and immune escape[4,7,12,15]. T-SLICE
269 represents a simple and effective *in vitro* 3-D system that mimics key features of the TME. By
270 growing a fibroblast monolayer and cancer cell spheroids between two glass coverslips, T-
271 SLICE creates physio-chemical gradients in which we observe hypoxic response with
272 diminutions in cellular proliferation and viability, as well as corresponding loss of MMP moving
273 from the periphery towards the middle of T-SLICE.

274 In our studies, we worked with three tumor cell lines representing breast and ovarian
275 cancer. Although the degree of the physio-chemical gradients varied for each, they each
276 demonstrated hypoxic responses, with spatially correlated cellular proliferation, apoptosis (loss
277 of mitochondrial transmembrane potential), and viability. Compered to cancer models that rely
278 on extrinsically imposed oxygen gradients[16,17], a cell-driven gradient generated by metabolic
279 demand has a better chance of faithfully reflecting the TME of different tumour types and
280 geometries. Here we did not measure oxygen tension within the T-SLICE to evidence hypoxia,
281 instead we relied on EF5, cell viability and proliferation markers to detect the cellular hypoxic
282 response. Trends described, including increasing hypoxic response as well as reduced viability
283 and cell proliferation moving towards the center of T-SLICE, have been observed in other cell-
284 driven hypoxic cancer models[18,19].

285 We confirmed that the strength and area of hypoxic zone within T-SLICE can be
286 increased by reducing the device gap height from 700 to 300 μm. A minimum gap height must

287 be maintained to accommodate the spheroids (<150 μm diameter), but by increasing the diameter
288 of T-SLICE this increases the diffusion distance from periphery to middle thereby decreasing the
289 hypoxic area. This effectively recapitulates TMEs and hypoxia as it would occur in different-
290 sized tumors or at varying distances from blood vessels. By comparison, in spheroid culture, an
291 increase in hypoxic effect can only be achieved with more cells and larger spheroid diameters
292 which will also directly impair the ability to observe cell behaviors within the spheroids. Using
293 T-SLICE, physio-chemical gradients can be uncoupled from tissue architecture, therefore
294 making it possible to observe cellular events within a comparable TME from a much larger
295 spheroid, or a centimeter sized human tumour.

296 With increasing focus on personalized and precision medicine approaches to cancer
297 therapy, there is an urgent need to develop faithful and high-throughput systems that can be
298 efficiently adopted by life science research laboratories around the world. Conventional 2-D
299 culture and model organisms have been informative for understanding mechanism and disease
300 processes; however, 2-D systems lack a tumor's structural and physio-chemical characteristics.
301 Model organisms, including xenografted or humanized mice, are excellent tools to study cancer
302 in a complex microenvironment, but lack a human immune system, require extensive workup
303 and monitoring[20], and can be quite heterogeneous. Microfluidic platforms in combination with
304 3-D culture systems allow a small number of explanted tumor, immune and accessory cells to be
305 grown and studied, but their complex set-ups make them out of reach for most life science
306 laboratories[21]. Moreover, endpoint sample recovery can be challenging in sealed microfluidic
307 devices, thus further impairing their usability as a standard model to study cancer biology. In
308 contrast, T-SLICE can be easily assembled using components that can be readily made to fit
309 inside standard cell culture vessels (e.g. 6-well plate), allows high-throughput tumor studies with

310 continuous monitoring capability in a broadly affordable and feasible way. The transparency of
311 T-SLICE combined with thin cell layers enable brightfield and fluorescent live-cell imaging. By
312 simply lifting the T-SLICE with forceps, selected portions of cells or the entire culture can be
313 harvested for endpoint histologic analysis using standard staining protocol, all without disrupting
314 the overall spatial arrangement of cells.

315 An advantage that T-SLICE shares with microfluidic culture platforms is the low cell
316 number needed to establish culture and strong paracrine signalling gradients due to the small
317 culture volume. With T-SLICE, fewer than a million cells harvested from patients can be
318 cultured within an environment that mimics the TME of a centimeter sized tumour. Such models
319 using conventional spheroid culture would require several magnitudes more cells and will not be
320 imageable. With a small number of cells, features and interventions can be studied with iteration
321 in adjacent wells of the same plate. Limitations in harvesting sufficient cells to study
322 interventions are circumvented in T-SLICE, making it feasible to routinely incorporate precious
323 patient biopsy samples for therapy screening. Patient avatars could be created to test various
324 strategies and combinations[22,23]. We show that simple adjustments, like changing the gap height,
325 have predictable impacts on the hypoxic gradient; this is relevant because oxygen availability
326 varies even within the same tumor[22,23]. Presently, the hypoxia in T-SLICE is driven primarily by
327 the fibroblast monolayer; however, relative proportions of the tumor, stromal and other cells
328 should be carefully considered and included to reflect specific applications of T-SLICE. Oxygen,
329 nutrients, small molecules, and immune cells will be subject to the challenges created in T-
330 SLICE, just as they are in a tumor. Thus, by designing studies which accurately simulate TMEs
331 within T-SLICE, we can more faithfully capture *in vivo* like drug responses in pre-clinical drug
332 screening, promoting success in the later stages of clinical trials.
333

334 **Acknowledgements**

335 The authors thank Ms. Sarah Nersesian and Dr. Naeimeh Jafari for technical assistance and
336 discussions on T-SLICE development. MPT and ND are trainees in the Cancer Research
337 Training Program of the Beatrice Hunter Cancer Research Institute, with funds for MPT
338 provided by the Bruce and Dorothy Rosetti Endowment through the Dalhousie Medical Research
339 Foundation and funds for ND provided by the Helyer/Williams Studentship. MPT is funded by a
340 CIHR Canadian Graduate Scholarship - Masters and a Nova Scotia Graduate Scholarship. ND is
341 supported by a Canadian Graduate Scholarship (Masters; NSERC) and a Genomics in Medicine
342 Scholarship through the Dalhousie Medical Research Foundation. JEB is the Dalhousie Medical
343 Research Foundation Cameron Cancer Scientist. We acknowledge the support of the
344 Government of Canada's New Frontiers in Research Fund (NFRF), [NFRFE-2019-00415] and
345 the OvCAN models consortium for funding this research. We thank Dr. Madhuri Koti (Queen's
346 University) for the ID8-Trp53$^{-/-}$ cell line.

347

348 **Author Contributions**

349 T-SLICE model and study was conceptualized by MPT, ND, JEB, BML; experiments were
350 designed, conducted, and validated by MPT and ND. Data analysis was conducted by MPT, ND,
351 JEB, BML. The manuscript was written by MPT, ND, JEB, and BML, reviewed, edited, and
352 approved by all authors.

353

354 **Declaration of interests**

355 The authors declare that no competing interests exist.

356

Inclusion and Diversity statement

Dalhousie University is located on the ancestral and unceded territory of the Mi'kmaq peoples.

We strive toward understanding, inclusion and awareness.

361 **References**

362 1 Emon, B., Bauer, J., Jain, Y., Jung, B. & Saif, T. Biophysics of Tumor Microenvironment
363 and Cancer Metastasis - A Mini Review. *Computational and Structural Biotechnology*
364 *Journal* **16**, 279-287, doi:10.1016/j.csbj.2018.07.003 (2018).

365 2 Balkwill, F. R., Capasso, M. & Hagemann, T. The tumor microenvironment at a glance.
366 *Journal of Cell Science* **125**, 5591-5596, doi:10.1242/jcs.116392 (2012).

367 3 Imparato, G., Urciuolo, F. & Netti, P. A. In vitro three-dimensional models in cancer
368 research: a review. *International Materials Reviews* **60**, 297-311,
369 doi:10.1179/1743280415y.0000000003 (2015).

370 4 Petrova, V., Annicchiarico-Petruzzelli, M., Melino, G. & Amelio, I. The hypoxic tumour
371 microenvironment. *Oncogenesis* **7**, doi:10.1038/s41389-017-0011-9 (2018).

372 5 Jing, X. *et al.* Role of hypoxia in cancer therapy by regulating the tumor
373 microenvironment. *Molecular Cancer* **18**, doi:10.1186/s12943-019-1089-9 (2019).

374 6 Carmona-Fontaine, C. *et al.* Metabolic origins of spatial organization in the tumor
375 microenvironment. *Proceedings of the National Academy of Sciences* **114**, 2934-2939,
376 doi:10.1073/pnas.1700600114 (2017).

377 7 Abou Khouzam, R. *et al.* Tumor Hypoxia Regulates Immune Escape/Invasion: Influence
378 on Angiogenesis and Potential Impact of Hypoxic Biomarkers on Cancer Therapies.
379 *Frontiers in Immunology* **11**, doi:10.3389/fimmu.2020.613114 (2021).

380 8 Wong, C. H., Siah, K. W. & Lo, A. W. Estimation of clinical trial success rates and
381 related parameters. *Biostatistics* **20**, 273-286, doi:10.1093/biostatistics/kxx069 (2019).

382 9 Spagnolo, F. *et al.* Treatment beyond progression with anti-PD-1/PD-L1 based regimens
383 in advanced solid tumors: a systematic review. *BMC Cancer* **21**, doi:10.1186/s12885-
384 021-08165-0 (2021).

385 10 Walton, J. *et al.* CRISPR/Cas9-Mediated Trp53 and Brca2 Knockout to Generate
386 Improved Murine Models of Ovarian High-Grade Serous Carcinoma. *Cancer Research*
387 **76**, 6118-6129, doi:10.1158/0008-5472.Can-16-1272 (2016).

388 11 Koch, C. J. in *Redox Cell Biology and Genetics Part A Methods in Enzymology* 3-31
389 (2002).

390 12 Bhandari, V. *et al.* Molecular landmarks of tumor hypoxia across cancer types. *Nature*
391 *Genetics* **51**, 308-318, doi:10.1038/s41588-018-0318-2 (2019).

392 13 Zhao, X. *et al.* Hypoxia-Inducible Factor 1-α (HIF-1α) Induces Apoptosis of Human
393 Uterosacral Ligament Fibroblasts Through the Death Receptor and Mitochondrial
394 Pathways. *Medical Science Monitor* **24**, 8722-8733, doi:10.12659/msm.913384 (2018).

395 14 Hanahan, D. Hallmarks of Cancer: New Dimensions. *Cancer Discovery* **12**, 31-46,
396 doi:10.1158/2159-8290.Cd-21-1059 (2022).

397 15 Busk, M., Overgaard, J. & Horsman, M. R. Imaging of Tumor Hypoxia for Radiotherapy:
398 Current Status and Future Directions. *Seminars in Nuclear Medicine* **50**, 562-583,
399 doi:10.1053/j.semnuclmed.2020.05.003 (2020).

16 Orcheston-Findlay, L., Hashemi, A., Garrill, A. & Nock, V. A microfluidic gradient generator to simulate the oxygen microenvironment in cancer cell culture. *Microelectronic Engineering* **195**, 107-113, doi:10.1016/j.mee.2018.04.011 (2018).

17 Nam, H., Funamoto, K. & Jeon, J. S. Cancer cell migration and cancer drug screening in oxygen tension gradient chip. *Biomicrofluidics* **14**, doi:10.1063/5.0011216 (2020).

18 Mosadegh, B. *et al.* A paper-based invasion assay: Assessing chemotaxis of cancer cells in gradients of oxygen. *Biomaterials* **52**, 262-271, doi:10.1016/j.biomaterials.2015.02.012 (2015).

19 Rodenhizer, D., Dean, T., Xu, B., Cojocari, D. & McGuigan, A. P. A three-dimensional engineered heterogeneous tumor model for assessing cellular environment and response. *Nature Protocols* **13**, 1917-1957, doi:10.1038/s41596-018-0022-9 (2018).

20 Walsh, N. C. *et al.* Humanized Mouse Models of Clinical Disease. *Annual Review of Pathology: Mechanisms of Disease* **12**, 187-215, doi:10.1146/annurev-pathol-052016-100332 (2017).

21 Hammel, J. H., Cook, S. R., Belanger, M. C., Munson, J. M. & Pompano, R. R. Modeling Immunity In Vitro: Slices, Chips, and Engineered Tissues. *Annual Review of Biomedical Engineering* **23**, 461-491, doi:10.1146/annurev-bioeng-082420-124920 (2021).

22 Yoshida, G. J. Applications of patient-derived tumor xenograft models and tumor organoids. *Journal of Hematology & Oncology* **13**, doi:10.1186/s13045-019-0829-z (2020).

23 Voabil, P. *et al.* An ex vivo tumor fragment platform to dissect response to PD-1 blockade in cancer. *Nature Medicine* **27**, 1250-1261, doi:10.1038/s41591-021-01398-3 (2021).

425 **Figures and Captions**

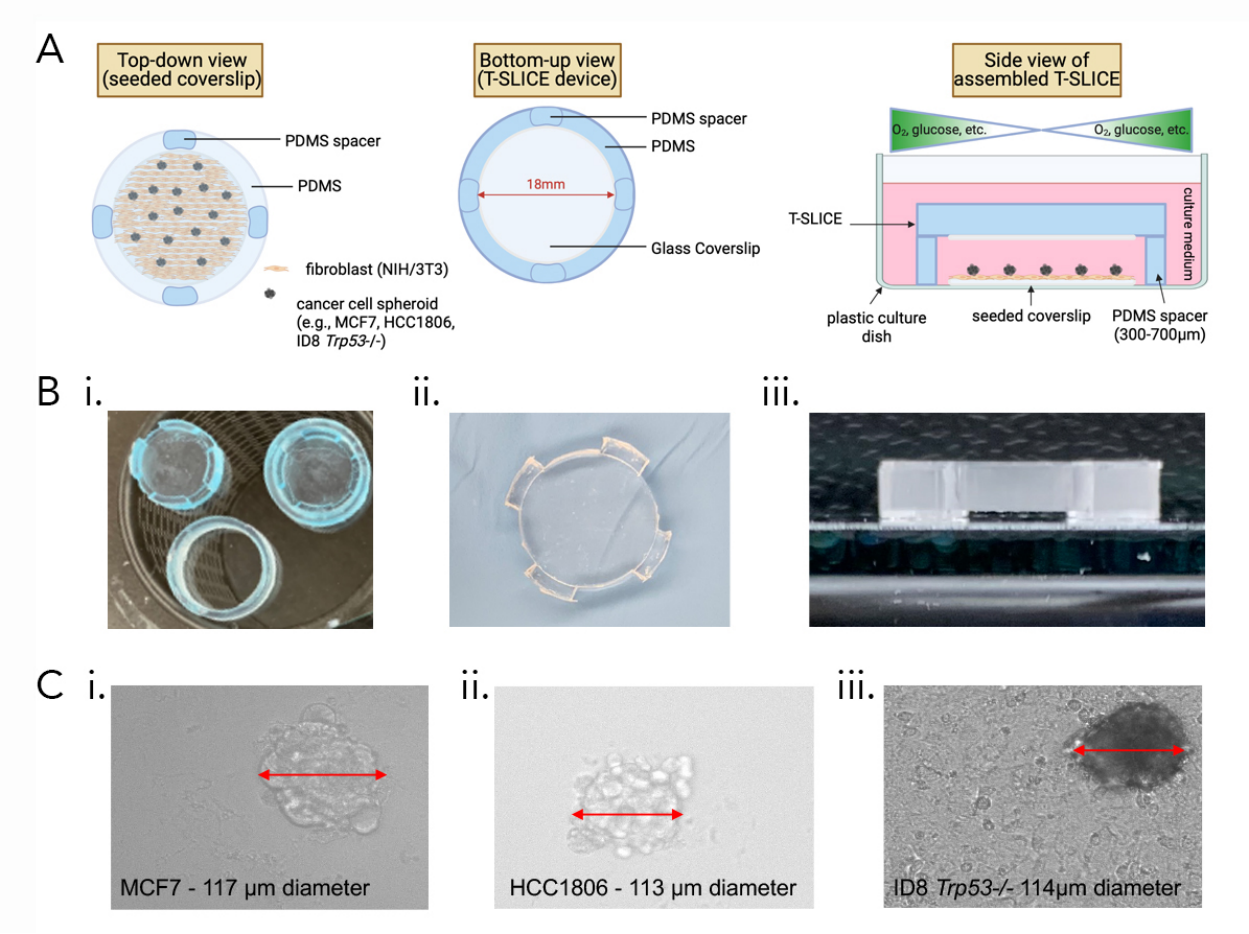

426

427 **Figure 1: T-SLICE Schematic, Design & Assembly. (A)** Top, bottom and side-view
428 schematic of T-SLICE demonstrating the placement of chips and resulting physio-chemical
429 gradients. (B) photograph of (i) two-part T-SLICE mold (shown both assembled, top right, and
430 in component ring and insert pieces (bottom and top left); (ii) top-down and (iii) side view of
431 assembled T-SLICE. (C) photographs depicting tumor cell line spheroids atop fibroblast
432 monolayers imaged through a T-SLICE chip: (i) MCF7; (ii) HCC1806; (iii) ID8 *Trp53*$^{-/-}$.

433

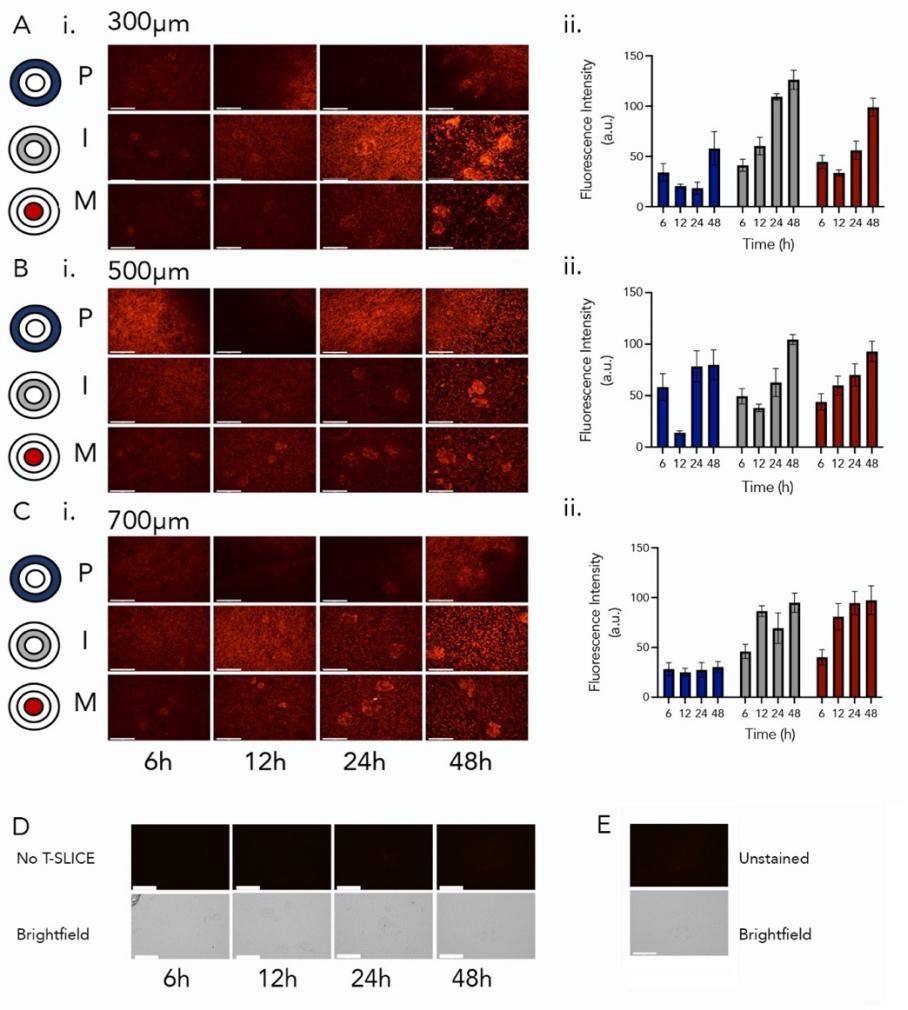

Figure 2: T-SLICE generates hypoxic gradients from the periphery to the center. MCF7 spheroids were seeded atop a fibroblast monolayer for 6, 12, 24 or 48h. Thereafter, cells were fixed and stained with EF5 to ascertain hypoxic responses (A-C). (i) photographs; (ii) fluorescence quantifications. (D and E) control wells either did not have a T-SLICE installed (D) or did not include dye (E). P, periphery (blue); M, middle (grey); I, intermediate (red); a.u., Arbitrary units. Scale bars represent 275 µm. Data are representative of three technical replicates with measurements of fluorescence intensity in three fields of view for each zone ($p<0.0001$, error bars represent standard deviation (SD)).

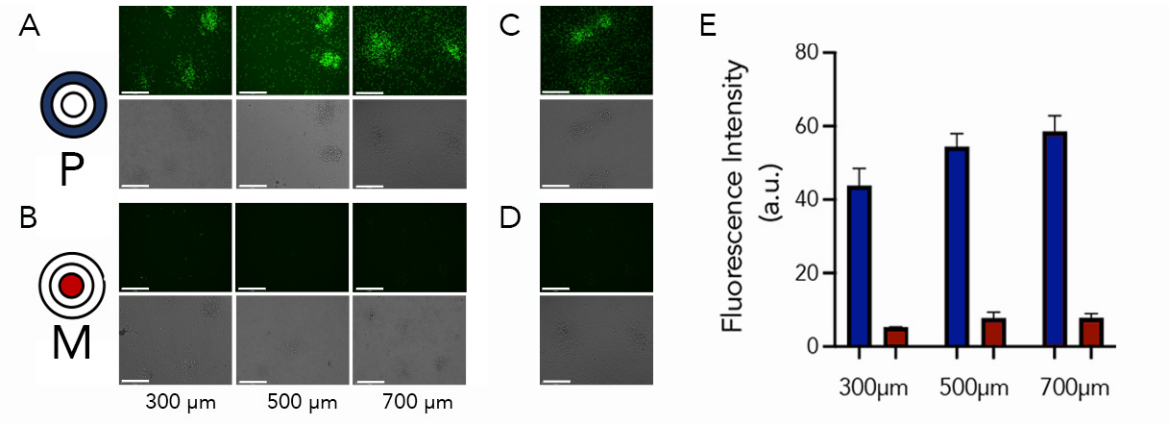

Figure 3. Cellular proliferation is halted in the middle region of T-SLICE. MCF-7 cells were seeded on a fibroblast monolayer in T-SLICE in the presence of EDU. After 72h incubation, cellular proliferation (EDU incorporation) was ascertained by fluorescence microscopy. (A) peripheral zone; (B) Middle zone; C) No T-SLICE control; D) unstained control; (E) quantification of fluorescence. a.u., Arbitrary units. Blue bars represent quantification from the peripheral zone; red bars represent quantification from the middle zone. Scale bars represent 275µm. Data are representative of three technical replicates with measurements of fluorescence intensity in three fields of view for each zone ($p<0.0001$, error bars represent SD).

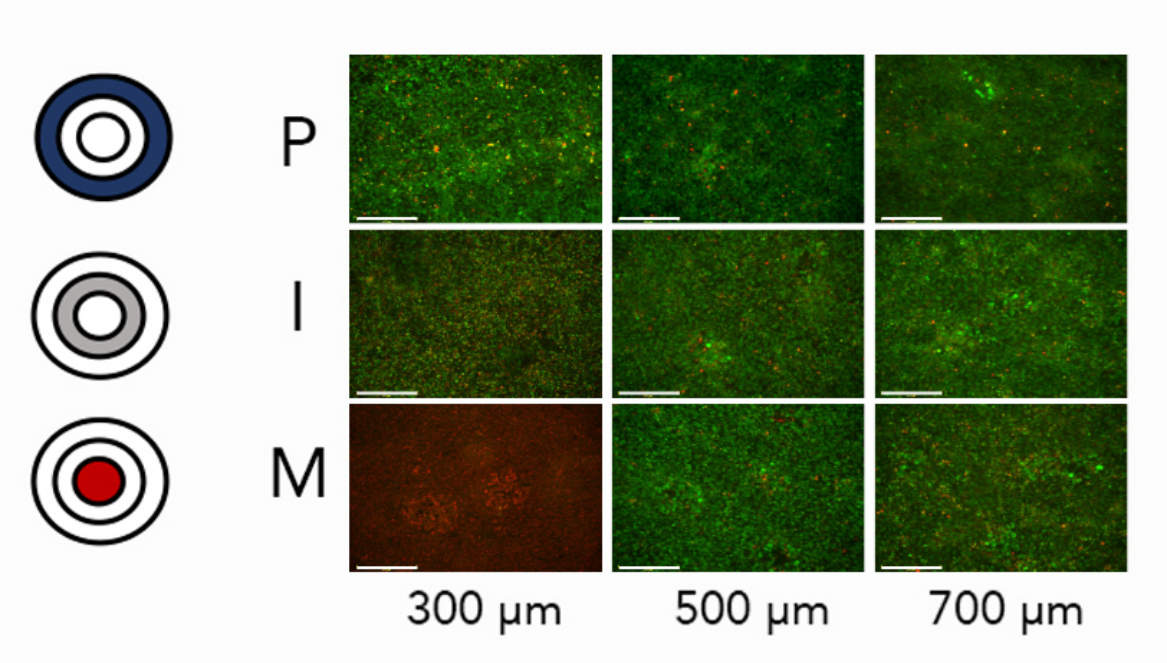

Figure 4: Cell viability is lost in the most hypoxic regions of T-SLICE. MCF7 spheroids were cultured in T-SLICE on a fibroblast monolayer for 72h, then stained with Calcein-AM and ethidium homodimer to visualize cell viability. Images are representative of three technical replicates and three fields of view for each T-SLICE zone. P, periphery; I, intermediate; M, middle.

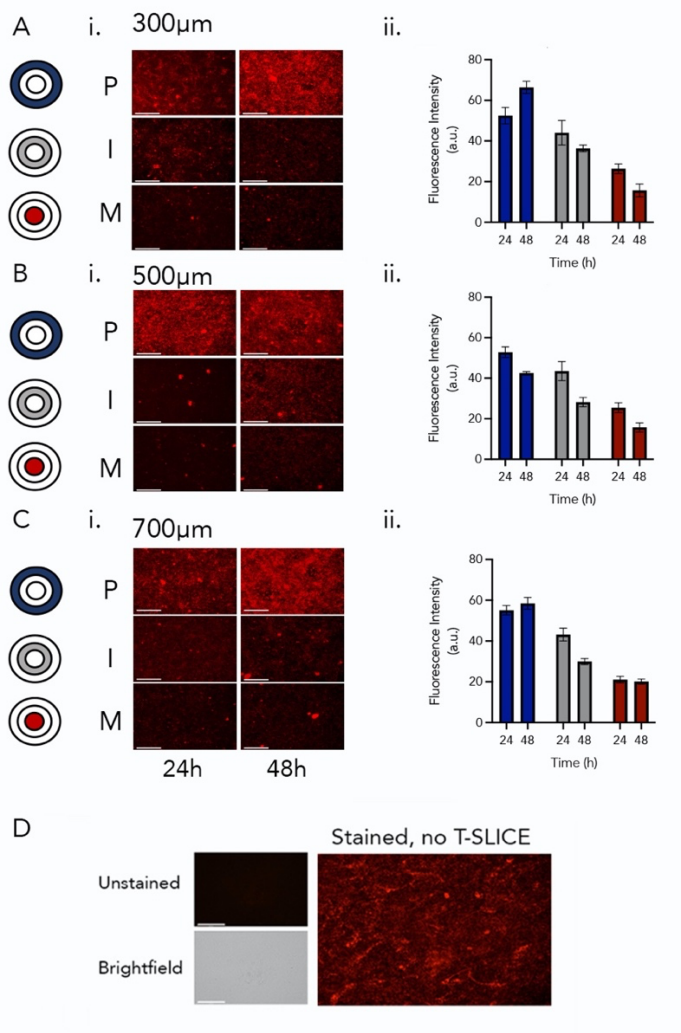

Figure 5. Mitochondrial trans-membrane potential is reduced in T-SLICE. MMP was measured using MitoView 633 staining after 24 or 48h in MCF7 cells. Significant diminishment was observed in the intermediate and middle zones compared to the periphery ($p<0.001$) with greater impact after 48h ($p<0.001$). (A-C) each of 300, 500 and 700 µm gap heights were tested. (i) representative images; and (ii) quantification are shown. (D) controls included unstained cells in T-SLICE, and stained cells with no T-SLICE. P, periphery (blue); M, middle (grey); I, intermediate (red); a.u., Arbitrary units. Scale bars represent 275µm. Data are representative of three technical replicates with measurements of fluorescence intensity in three fields of view for each zone ($p<0.001$ after 24h, $p<0.0001$ after 48h, error bars represent SD).

Supplemental Information:

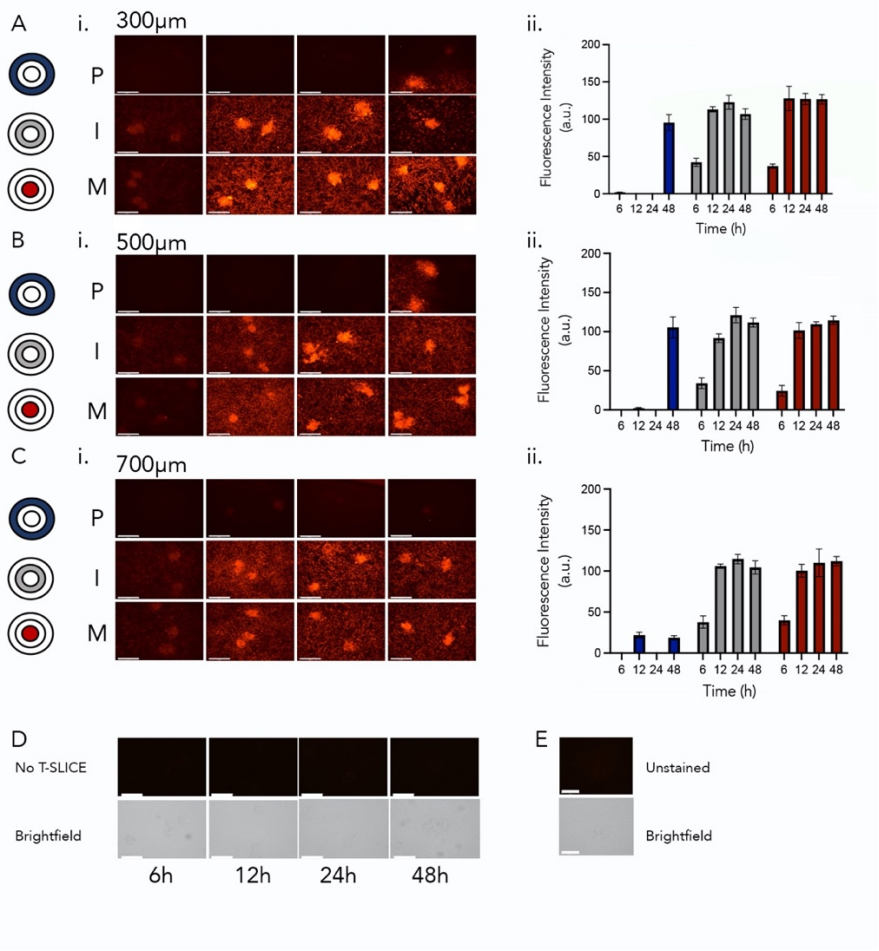

Supplementary Figure 1: T-SLICE hypoxic gradients from the periphery to the center in a second cell line (related to Figure 2). HCC1806 spheroids were seeded atop a fibroblast monolayer for 6, 12, 24 or 48h. Thereafter, cells were fixed and stained with EF5 to ascertain hypoxic responses (A-C). (i) photographs; (ii) fluorescence quantifications. (D and E) control wells either did not contain dye (D) or did not have a T-SLICE chip installed I. P, periphery; M, middle; I, intermediate. Scale bars represent 275µm. Data are representative of three technical replicates with measurements of fluorescence intensity in three fields of view for each zone ($p<0.0001$, error bars represent SD).

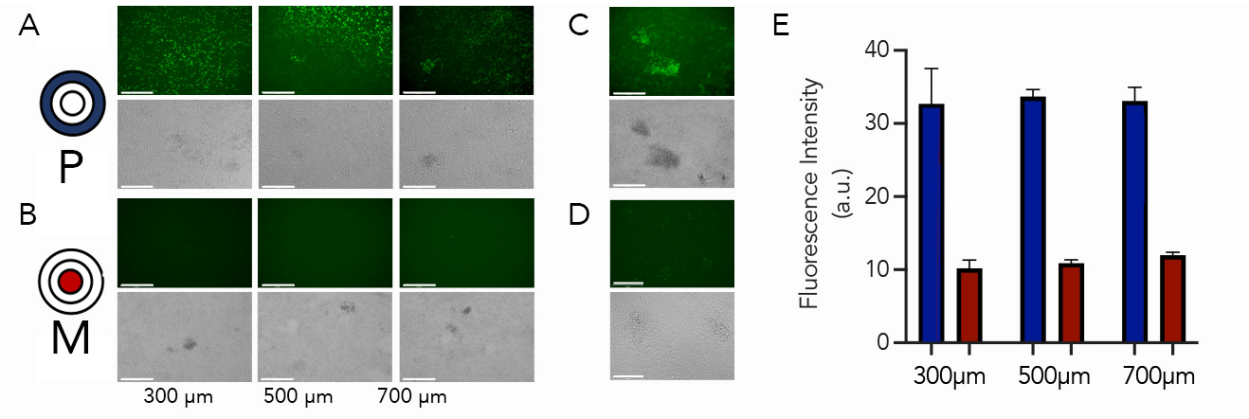

Supplementary Figure 2: Cellular proliferation is slowed in a second cell line model in T-SLICE. HCC1806 cells were seeded on a fibroblast monolayer in T-SLICE in the presence of EDU. After 72h incubation, cellular proliferation (EDU incorporation) was ascertained by fluorescence microscopy. (A) peripheral zone; (B) Middle zone; C) No T-SLICE control; D) unstained control; (D) quantification of fluorescence. a.u., Arbitrary units. Scale bars represent 275µm. Data are representative of three technical replicates with measurements of fluorescence intensity in three fields of view for each zone ($p<0.0001$, error bars represent SD).

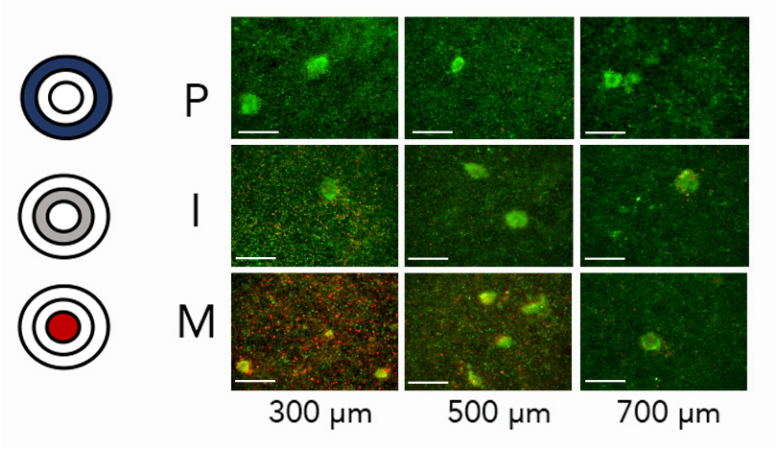

Supplementary Figure 3: Cellular viability is lost in the most hypoxic regions of T-SLICE in a second cell line. ID8-Trp53$^{-/-}$ spheroids were cultured in T-SLICE on a fibroblast monolayer for 72h, then stained with Calcein-AM and ethidium homodimer to visualize cell viability. Images are representative of three technical replicates and three fields of view for each T-SLICE zone. P, periphery; I, intermediate; M, middle.

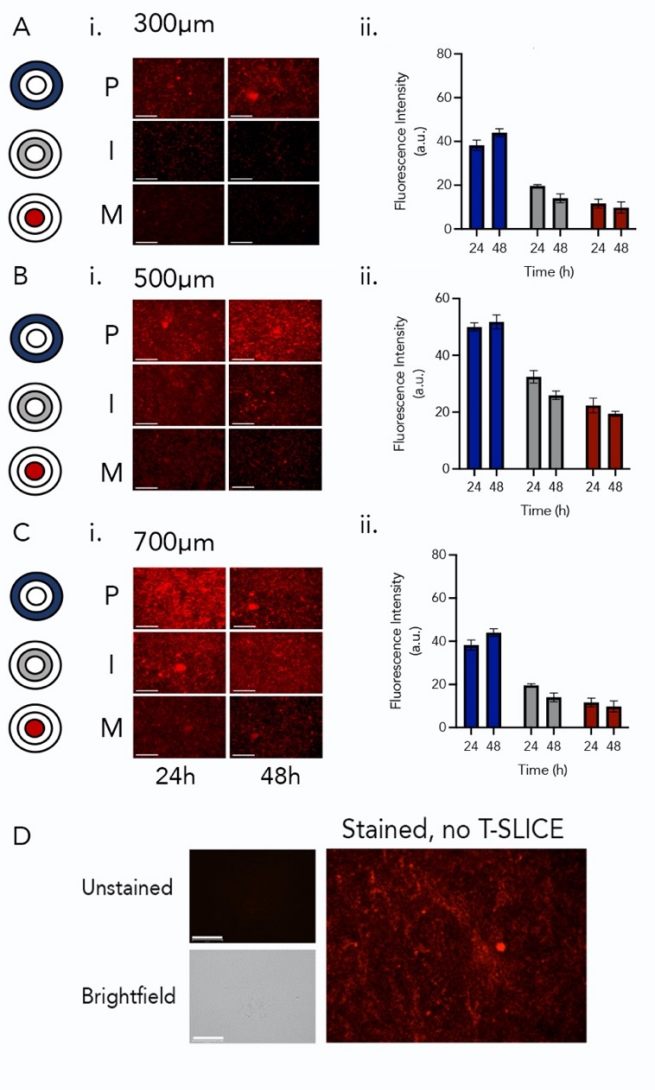

Supplementary Figure 4. MMP is reduced in T-SLICE in a second cell line. MMP was measured using MitoView 633 staining after 24 or 48h in ID8-Trp53-/- cells. (A-C) each of 300, 500 and 700 µm gap heights were tested. (i) representative images; and (ii) quantification are shown. (D) controls included unstained cells in T-SLICE, and stained cells with no T-SLICE. P, periphery (blue); M, middle (grey); I, intermediate (red); a.u., Arbitrary units. Scale bars represent 275 µm. Data are representative of three technical replicates with measurements of fluorescence intensity in three fields of view for each zone ($p<0.001$ after 24h, $p<0.0001$ after 48h, error bars represent SD).